ADAPTIVE EDGE DETECTORS FOR PIECEWISE SMOOTH DATA BASED ON THE MINMOD LIMITER

ANNE GELB AND EITAN TADMOR

Abstract. We are concerned with the detection of edges – the location and amplitudes of jump discontinuities of piecewise smooth data realized in terms of its discrete grid values. We discuss the interplay between two approaches. One approach, realized in the physical space, is based on local differences and is typically limited to low-order of accuracy. An alternative approach developed in our previous work [6] and realized in the dual Fourier space, is based on concentration factors; with a proper choice of concentration factors one can achieve higher-orders – in fact in [7] we constructed exponentially accurate edge detectors. Since the stencil of these highly-accurate detectors is global, an outside threshold parameter is required to avoid oscillations in the immediate neighborhood of discontinuities. In this paper we introduce an adaptive edge detection procedure based on a cross-breading between the local and global detectors. This is achieved by using the *minmod* limiter to suppress spurious oscillations near discontinuities while retaining high-order accuracy away from the jumps. The resulting method provides a family of robust, parameter-free edge-detectors for piecewise smooth data. We conclude with a series of one- and two-dimensional simulations.

To David Gottlieb, on his 60^{th} birthday, with friendship and appreciation

Contents

Date: April 19, 2005.

1991 *Mathematics Subject Classification.* 42A10, 42A50, 65T10.

Key words and phrases. Edge detection, concentration method, piecewise smoothness, local difference formulas, minmod algorithm.

Research was supported in part by NSF DMS #01-07428 (AG and ET), by NSF EAR #02-22327, CNS #03-24957 and NIH EB #02533-01 (AG) and by ONR #N00014-91-J-1076 and NSF #DMS04-07704 (ET). Part of the research was carried out while A. Gelb was visiting the Center for Scientific Computation and Mathematical Modeling (CSCAMM) at the University of Maryland, College Park.

1. Introduction and motivations

The detection of edges in images is an increasingly important area of research. Not only is the knowledge of the jump locations essential in high resolution reconstruction methods, e.g. [9, 15, 16], but there are many scientific applications in which the knowledge of the edges and their associated jump values are useful in of themselves. One classical example arises in magnetic resonance imaging (MRI) segmentation which enables various features of interest to be "separated" out for closer examination. Edge detection determines the boundaries of each particular region and classifies the type of region based on the jump value at the boundaries. Since the most relevant information is often found near the borders of each segmented region, it is imperative that edge detection is performed successfully. Furthermore, due to the cost of MRI, resolution is somewhat limited. Hence features in an image might be spread over as few as two pixel data points with the edges located extremely close together. Finally, computational efficiency and robustness are particularly relevant in the case of MRI since huge amounts of data must be processed in short periods of time.

In our previous work, [6, 7, 8], we describe an edge detection procedure which recovers the location and amplitudes of edges from spectral information provided either by the continuous spectral coefficients or the discrete ones based on equally spaced grid values in physical space. These detectors effectively resolve the jump function, $[f](x)$, so that edges are detected by separation. Specifically, the detectors "concentrate" near the $\mathcal{O}(1)$ scale of jump discontinuities which are effectively separated from the smooth regions where $[f](x) \sim 0$. This procedure offers a large family of edge detectors, each detector is associated with its own particular concentration factors. The prescribed procedure is computationally efficient and robust; there are, whoever, two major drawbacks. First, in order to "pinpoint" the edges one has to introduce an outside threshold parameter to quantify the "large" jumps, i.e., those with $[f](x) \gg \mathcal{O}(\Delta x)$, implying that the edge detection method is inherently problem dependent [7]. Second, oscillations form in the neighborhood of the jump discontinuities. The particular behavior of these oscillations depends on the specific concentration factors used. Therefore it can be difficult to distinguish what constitutes a true jump discontinuity as opposed to an oscillating artifact, particularly when several jump discontinuities are located in the same neighborhood, i.e. when there is limited resolution for the problem.

In this paper we develop an adaptive, parameter-free edge detection procedure based on the *nonlinear* limiting of low- and high-order concentration factors. Here, we tie in the possibility of using "local" edge detectors based on equally spaced grid points to "global" concentration methods based on pseudo-spectral coefficients. The paper is organized as follows: In §2 we discuss local edge detectors based on equally spaced grid points in physical space. In §3 we review the concentration method in dual space and describe low- and high-order concentration factors. We also establish the consistency of both, the local and global approaches. An adaptive, parameter-free edge detection procedure is introduced in §4: here we use nonlinear limiting procedure, based on the so-called minmod limiter, to retain the high-order in smooth regions while "limiting" the high-order spurious oscillations in the neighborhoods of the jumps by the less oscillatory low-order detectors. Finally, §5 contains numerical examples of two dimensional applications of our new adaptive method.

Although we limit our analysis to periodic piecewise smooth functions on $[-\pi, \pi)$, we note that our method is easily adapted for the general intervals and that in two dimensions, edge detection is performed one dimension at a time.

2. Local detection of edges by (undivided) differences

Consider a periodic piecewise smooth function $f(x)$ on $[-\pi, \pi)$ for which we wish to identify the points of discontinuity. The corresponding jump function can be defined as $[f](x) := f(x+) - f(x-)$, where $f(x\pm)$ are the right and left side limits of the function at x. Suppose we are given discrete grid point values of $f(x)$, with $f_j := f(x_j)$ on equidistant points $x_j = -\pi + j\Delta x$, $j = 0, \cdots, 2N$, where $\Delta x = \frac{2\pi}{2N+1}$. A jump discontinuity at $x = \xi$ is identified by its enclosed grid cell, $x_j \le \xi \le x_{j+1}$, and is characterized by the asymptotic statement

$$\Delta f_{j+\frac{1}{2}} := f_{j+1} - f_j = \begin{cases} [f](\xi) + \mathcal{O}(\Delta x) & \text{for } j = j_\xi : \xi \in [x_j, x_{j+1}] \\ \mathcal{O}(\Delta x) & \text{for } j \neq j_\xi. \end{cases} \tag{2.1}$$

From (2.1), it is clear that the function $f(x)$ experiences a jump discontinuity at every grid point x_j, and that the determination of what constitutes a jump is based on an asymptotic statement which is inherently a user dependent. It is reasonable, for instance, to assign jump values to points corresponding to those $x_{j+\frac{1}{2}}$'s such that $|\Delta f_{j+\frac{1}{2}}| \gg \mathcal{O}(\Delta x)$. Therefore the local differences (2.1) can be viewed as an edge detection method of first order.

To demonstrate the application of (2.1), consider the following examples

$$f_a(x) := \begin{cases} (\frac{x+\pi}{\pi})^5, & x < 0, \\ (\frac{x-\pi}{\pi})^5, & x > 0. \end{cases} \quad ; \qquad f_b(x) := \begin{cases} \sin(x+1)^7 & x < -\frac{\pi}{2}, \\ (\frac{x}{\pi})^3 - \sin(\frac{9x}{2}) + 1, & -\frac{\pi}{2} < x < \frac{\pi}{2}, \\ \sin(x-1)^7, & x > \frac{\pi}{2}. \end{cases} \tag{2.2}$$

Figure 2.1 displays these piecewise smooth functions on equally spaced grid points.

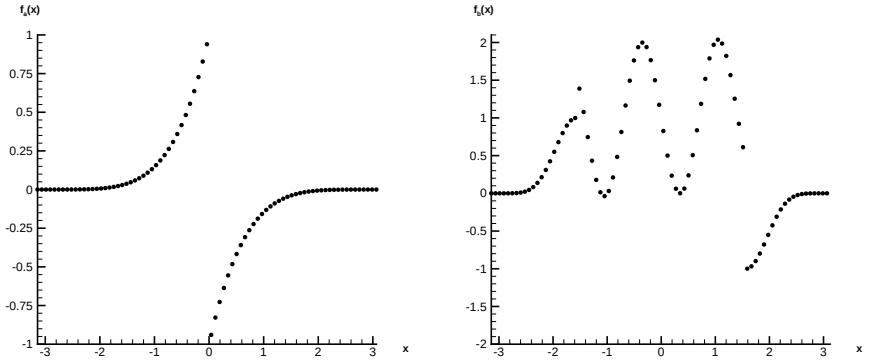

Figure 2.1: (a) $[f_a](x)$ and (b) $[f_b](x)$ on $N = 80$ equally spaced grid points.

The corresponding jump functions are

$$[f_a](x) := \begin{cases} -2, & x = 0, \\ 0 & x \neq 0. \end{cases} \quad ; \qquad [f_b](x) := \begin{cases} .582, & x = -\frac{\pi}{2}, \\ -1.418, & x = \frac{\pi}{2}, \\ 0 & x \neq \pm\frac{\pi}{2}. \end{cases} \tag{2.3}$$

Figures 2.2 and 2.3 demonstrate the convergence of the local first order difference method (2.1) to the jump function $[f](x)$.

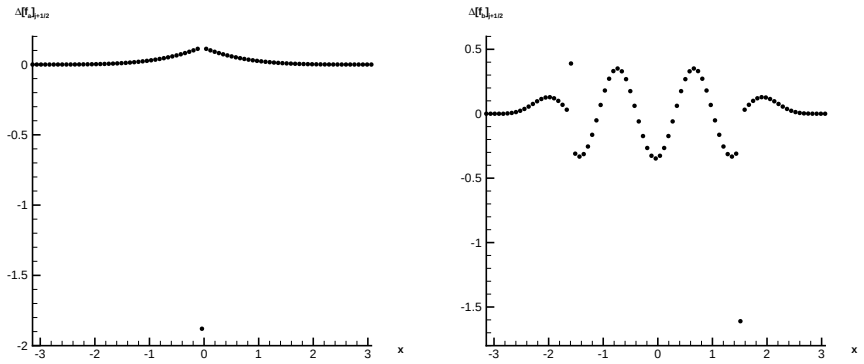

Figure 2.2: Application of (2.1) for $N = 80$ to approximate (a) $[f_a](x)$ and (b) $[f_b](x)$.

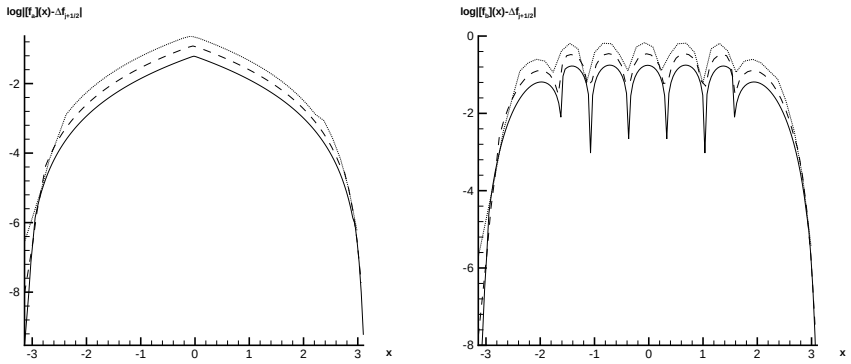

Figure 2.3: The logarithmic error of the difference formula (2.1) for (a) $[f_a](x)$ and (b) $[f_b](x)$, with $N = 40, 80$, and 160.

While the simple construction of differences (2.1) might suffice for determining the jump discontinuities for functions like $[f_a](x)$ and $[f_b](x)$, it is not difficult to imagine that distinguishing a jump discontinuity from a smooth region might become more complicated for functions with higher variation or smaller scales. Therefore we seek an edge detection method that yields higher order convergence to zero away from the singular support of the function.

Following (2.1), we consider higher order local difference formulas of order $2p + 1$ to obtain faster convergence in the smooth regions of f. For example, the first few higher order difference formulas yield

$$\begin{aligned} \Delta^1 f_{j+\frac{1}{2}} &:= f_{j+1} - f_j, \\ \Delta^3 f_{j+\frac{1}{2}} &:= -f_{j+2} + 3f_{j+1} - 3f_j + f_{j-1}, \\ \Delta^5 f_{j+\frac{1}{2}} &:= f_{j+3} - 5f_{j+2} + 10f_{j+1} - 10f_j + 5f_{j-1} - f_{j-2}, \end{aligned} \tag{2.4}$$

TABLE 1. Short table of coefficients for $\Delta^{2p+1} f_{j+\frac{1}{2}}$.

$2p+1 \backslash j+l$	j+5	j+4	j+3	j+2	j+1	j	j-1	j-2	j-3	j-4
1					1	-1				
3				-1	3	-3	1			
5			1	-5	10	-10	5	-1		
7		-1	7	-21	35	-35	21	-7	1	
9	1	-9	36	-84	126	-126	84	-36	9	-1

and in general we have

$$\Delta^{2p+1} f_{j+\frac{1}{2}} = \sum_{l=-p}^{p} (-1)^{l+1} \left(\begin{array}{c} 2p+1 \\ p-|l| \end{array} \right) f_{j+1+l}. \tag{2.5}$$

The coefficients for the first few $\Delta^{2p+1} f_{j+\frac{1}{2}}$ are displayed in table 2.1. Away from the neighborhoods of discontinuities of $f(x)$, the sum (2.5) is of order $\mathcal{O}(\Delta x)^{2p+1}$. We now wish to determine its behavior in the neighborhoods of the jump discontinuities, and then use the results to develop local edge detectors of odd orders (we omit the even order difference formulas which require non-symmetric stencils around $x_{j+\frac{1}{2}}$).

To motivate our derivation of a local edge detection formula, let us examine the application of $\Delta^5 f_{j+\frac{1}{2}}$; the results of examples (2.2) are displayed in figure 2.4.

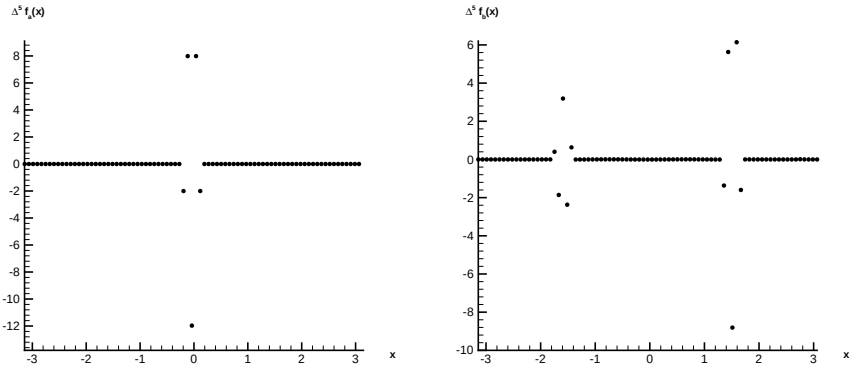

Figure 2.4: Application of $\Delta^5 f_{j+\frac{1}{2}}$ using $N = 80$ points to (a) $[f_a](x)$ and (b) $[f_b](x)$.

A simple computation based on (2.4) yields, in agreement with figure 2.4,

$$\Delta^5 f_{j+\frac{1}{2}} \sim \begin{cases} 6[f](\xi), & \text{if } \xi \in [x_j, x_{j+1}], \\ -4[f](\xi), & \text{if } \xi \in [x_{j-1}, x_j] \cup [x_{j+1}, x_{j+2}], \\ [f](\xi), & \text{if } \xi \in [x_{j-2}, x_{j-1}] \cup [x_{j+2}, x_{j+3}], \\ \mathcal{O}(\Delta x)^5, & \text{otherwise.} \end{cases} \tag{2.6}$$

It is evident from (2.6) that a local edge detection procedure can be developed from the general difference formula (2.5) that can identify both the location and the magnitudes of the jump discontinuities of piecewise smooth $f(x)$. Specifically, the (undivided) differences are

$\mathcal{O}(\Delta x)^{2p+1}$ in smooth regions, outside the immediate neighborhoods of a jumps, whereas within the symmetric $2p$-cells neighborhood of such jumps located at, say, $x = \xi$, we have

$$\Delta^{2p+1} f_{j+l+\frac{1}{2}} = \begin{cases} (-1)^l q_{l,p}[f](\xi) + \mathcal{O}(\Delta x), & \text{if } |l| \le p, \\ \mathcal{O}(\Delta x)^{2p+1}, & \text{if } |l| > p, \end{cases} \tag{2.7}$$

where [11]

$$q_{l,p} = (-1)^l \sum_{k=0}^{p-|l|} \left(\begin{array}{c} 2p+1 \\ k \end{array} \right) (-1)^k = \left(\begin{array}{c} 2p \\ p+|l| \end{array} \right). \tag{2.8}$$

Hence we consider the local edge detector

$$T_N^{2p+1}[f](x) = \frac{1}{q_{0,p}} \Delta^{2p+1} f_{j+\frac{1}{2}}, \quad q_{0,p} = \left(\begin{array}{c} 2p \\ p \end{array} \right). \tag{2.9}$$

Letting $N \to \infty$, we have

$$T_N^{2p+1}[f](x) \to \begin{cases} (-1)^l \dfrac{q_{l,p}}{q_{0,p}}[f](\xi), & \text{if } x_{j-p} \le \xi \le x_{j+1+p},\ |l| \le p, \\ \\ 0, & \text{otherwise,} \end{cases}$$

implying that as $N \to \infty$, $T_N^{2p+1}[f](x)$ "concentrates" at the jump discontinuities of $f(x)$ Here the index $l = l_\xi$ traces the cell enclosing the jump so that $|\xi - x_{j\pm l} - \Delta x/2| \le \Delta x/2$. We refer to (2.10) as the local concentration property and we note the oscillatory behavior of $T_N^{2p+1}[f](x)$ is increasing with growing p's.

Figures 2.5 and 2.6 display the results for applying the fifth order local edge detection method (2.9) to determine the jump functions (2.3). It is clear that the neighborhood of each jump discontinuity consists of two cells on each side with

$$T_N^5[f](x) = \begin{cases} [f](\xi) + \mathcal{O}(\Delta x), & \text{if } \xi \in [x_j, x_{j+1}], \\ -\frac{2}{3}[f](\xi) + \mathcal{O}(\Delta x), & \text{if } \xi \in [x_{j-1}, x_j] \cup [x_{j+1}, x_{j+2}], \\ \frac{1}{6}[f](\xi) + \mathcal{O}(\Delta x), & \text{if } \xi \in [x_{j-2}, x_{j-1}] \cup [x_{j+2}, x_{j+3}], \\ \mathcal{O}(\Delta x)^5, & \text{otherwise.} \end{cases}$$

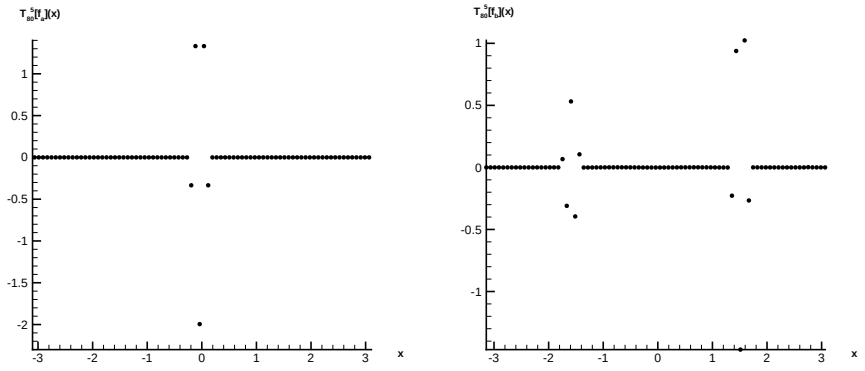

Figure 2.5: Application of $T_{80}^5[f](x_j)$ to approximate (a) $[f_a](x)$ and (b) $[f_b](x)$.

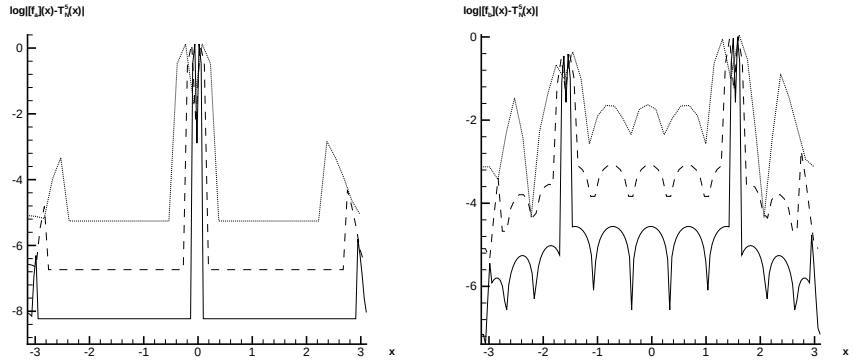

Figure 2.6: The logarithmic error of $T_N^5[f](x)$ for (a) $[f_a](x)$ and (b) $[f_b](x)$, with $N = 40, 80$, and 160.

Figure 2.7 compares the logarithmic errors of the local edge detector (2.9) for various orders p. We see that as a direct consequence of (2.10), higher order differencing lead to faster convergence away from the jump discontinuities, yet near the discontinuities, first order differencing is more advantageous, in the sense that no spurious oscillations are produced.

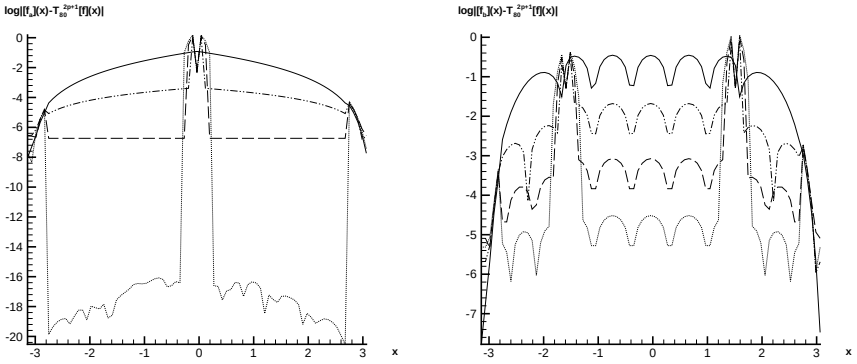

Figure 2.7: The logarithmic error of $T_{80}^{2p+1}[f](x_j)$ using $p = 0, \cdots, 3$ for (a) $[f_a](x)$ and (b) $[f_b](x)$.

3. Edge detection in the dual space: the global approach

In [6, 7, 8] we introduced a general family of edge detectors, based on the so-called concentration factors which are implemented in the dual Fourier space. The behavior of the edge detection procedure was linked to the type of concentration factor employed. The detectors, in the generic case, depend on the Fourier interpolant. Hence they lead to *global* edge detectors in the sense that their stencil involve all the discrete data. At the same time, we show below that the local edge detectors (2.9) can be viewed as special cases corresponding to specific trigonometric concentration factors. Let us first recall how the global concentration edge detection method is formulated (see [6] and [8]). Assume we are given discrete grid point data for a periodic piecewise smooth function $f(x)$ at $x_j = \frac{2\pi j}{2N+1}$, $j = 0, \cdots, 2N$. The discrete concentration

detector is defined as

$$\widetilde{T}_N^\tau[f](x) := \pi i \sum_{k=-N}^{N} sgn(k)\tau\Big(\frac{|k|\Delta x}{\pi}\Big)\widetilde{f}_k e^{ikx}, \tag{3.1}$$

where $\widetilde{f}_k$ are the usual pseudo-spectral coefficients,

$$\widetilde{f}_k = \frac{1}{N+1}\sum_{j=0}^{2N} f(x_j)e^{-ikx_j}, \tag{3.2}$$

and $\tau(s_k)$ are the discrete concentration factors,

$$\tau(s_k) = \sigma(s_k)sinc(\frac{\pi s_k}{2}), \qquad s_k := \frac{|k|\Delta x}{\pi}, \quad sinc(s) := \sin(s)/s. \tag{3.3}$$

Here $\sigma(s_k)$ are admissible concentration factors at our disposal; in [7], we have shown that the desired concentration property holds provided the following admissibility requirement is fulfilled.

Corollary 3.1. *Let $\sigma(\cdot) \in C^2[0,1]$ be admissible concentration factor so that $\int_0^1 \frac{\sigma(s)}{s}ds = 1$. Then concentration property*

$$\widetilde{T}_N^\tau[f](x) \to \begin{cases} [f](\xi), & \text{if } x = \xi, \\ 0 & \text{otherwise,} \end{cases} \qquad \text{as } N \to \infty,$$

holds for the edge detector (3.1) associated with the discrete concentration factors $\tau(s_k) = \sigma(s_k)sinc(\frac{\pi s_k}{2})$.

To gain a better insight on the behavior of such detectors, we rewrite (3.1) as

$$\widetilde{T}_N^\tau[f](x) = -\Delta x \sum_{j=0}^{2N} f(x_j) \sum_{k=1}^{N} \sigma\Big(\frac{k\Delta x}{\pi}\Big)\frac{\sin(k\Delta x/2)}{k\Delta x/2}\sin k(x-x_j), \tag{3.4}$$

and summation by parts then yields

$$\widetilde{T}_N^\tau[f](x) = \Delta x \sum_{j=0}^{N}(f(x_{j+1}) - f(x_j)) \sum_{k=1}^{N} \frac{\sigma(k\Delta x/\pi)}{k\Delta x}\cos k(x - x_{j+1/2}). \tag{3.5}$$

The summation on the right is dominated by the discontinuous cell(s) where $|f(x_{j+1}) - f(x_j)| \sim \mathcal{O}(1)$ while the contributions of the 'smooth' cells is negligible due to cancelations of oscillations. The precise statement of convergence to the jump function reads [8, §3]:

$$\widetilde{T}_N^\tau[f](x) = [f](\xi)\sum_{k=1}^{N}\frac{\sigma(k\Delta x/\pi)}{k}\cos k(x - \xi_{j+\frac{1}{2}}) + \mathcal{O}(\Delta x|\log \Delta x|). \tag{3.6}$$

Here $\xi_{j+\frac{1}{2}} := x_{j_\xi+\frac{1}{2}}$ is the midpoint identifying one discontinuous cell. Observe that such edge detectors identify *all* the jumps by concentrating around the support of the jump function at finitely many cells.

3.1. **Polynomial concentration factors: global edge detectors.** Several examples of admissible concentration factors were discussed in [6, 7]. We begin our discussion with the *polynomial* concentration factors,

$$\sigma_{2p+1}(s) := (2p+1)s^{2p+1}. \tag{3.7}$$

The corresponding τ_{2p+1} factors are $\tau_{2p+1}(s) = \sigma_{2p+1}(s)sinc(\pi s/2)$, and (3.5) yields

$$\widetilde{T}_N^{\tau_{2p+1}}[f](x) = \Delta x \sum_{j=0}^{2N} (f(x_{j+1}) - f(x_j)) \sum_{k=1}^{N} (2p+1)\Big(\frac{k\Delta x}{\pi}\Big)^{2p+1} \cdot \frac{\cos k(x - x_{j+\frac{1}{2}})}{k\Delta x}. \tag{3.8}$$

For the first order method, $p = 0$ in (3.8) reads

$$\widetilde{T}_N^{\tau_1}[f](x) = \Delta x \sum_{j=0}^{2N} (f(x_{j+1}) - f(x_j)) D_N(x - x_{j+\frac{1}{2}}), \tag{3.9}$$

where $D_N(y)$ is the usual Dirichlet sum, $D_N(y) = (1 + 2\sum_{k=1}^{N} \cos ky)/2\pi$. Hence, (3.9) tells us that the discrete concentration kernel associated with the first order polynomial factor (3.7) amounts to *interpolation of the first-order local differences*, $f(x_{j+1}) - f(x_j)$, at the intermediate grid points, $x_{j+\frac{1}{2}}$. In a similar fashion, concentration kernels associated with the higher order polynomial factors coincide with higher order derivatives of this interpolant. In fact, an equivalent formulation for (3.8) reads

$$\begin{aligned} \widetilde{T}_N^{\tau_{2p+1}}[f](x) &= (-1)^p \Big(\frac{2}{2N+1}\Big)^{2p} \sum_{k=-N}^{N} (2p+1)(ik)^{2p} \widetilde{g}_k e^{ikx} = \\ &= (-1)^p (2p+1)\Big(\frac{2}{2N+1}\Big)^{2p} \frac{d^{2p}}{dx^{2p}} \widetilde{T}_N^{\tau_1}[f](x), \end{aligned} \tag{3.10}$$

where $\widetilde{g}_k = \frac{1}{2N+1}\sum_{j=0}^{N}(f(x_{j+1}) - f(x_j))e^{-ikx_{j+\frac{1}{2}}}$ are the discrete Fourier coefficients of the interpolant of the differences we met above. Figures 3.1 and 3.2 display the results for applying (3.1) with a fifth order polynomial concentration factor (3.7).

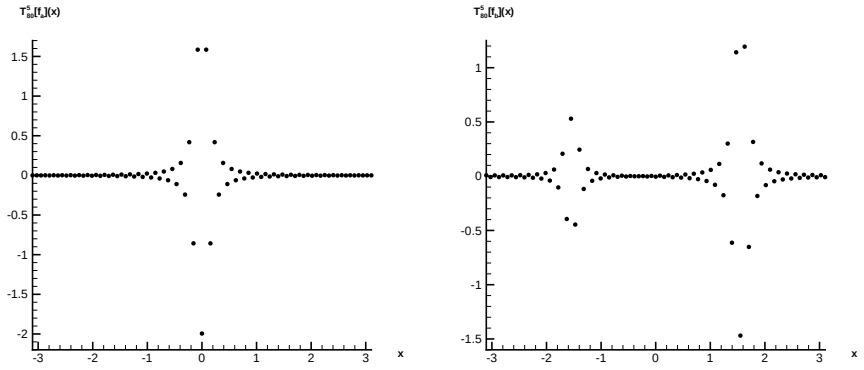

Figure 3.1: Application of $\widetilde{T}_{80}^{\tau_5}[f](x)$ with (3.7) to approximate (a) $[f_a](x)$ and (b) $[f_b](x)$.

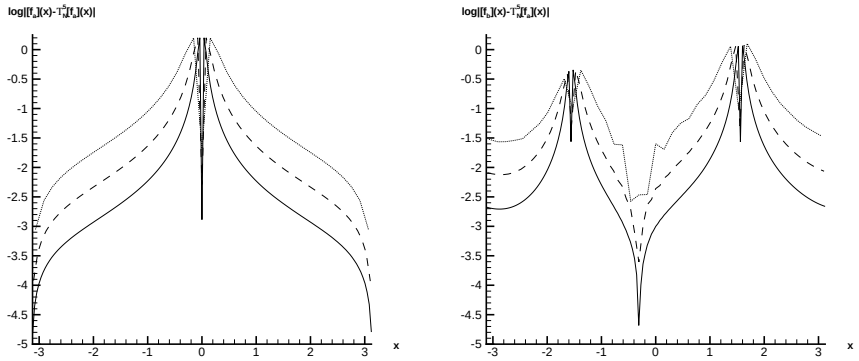

Figure 3.2: The logarithmic error of $\widetilde{T}_N^{\tau_5}[f](x)$ with (3.10) for (a) $[f_a](x)$ and (b) $[f_b](x)$, with $N = 40, 80$, and 160.

We note that resulting edge detectors using the polynomial concentration factors are *global* in the sense that they depend on the global interpolant of f, for $\widetilde{T}_N^{\tau_{2p+1}}[f](x) = \big(\widetilde{T}_N^{\tau_1}[f]\big)^{(2p)}(x)$; the corresponding stencil involves all th grid values on the 2π interval. It is interesting to compare these results to the local fifth order edge detection method displayed in figures 2.5 and 2.6. The global nature of (3.1) is clearly indicated by the oscillations that exist throughout the domain.

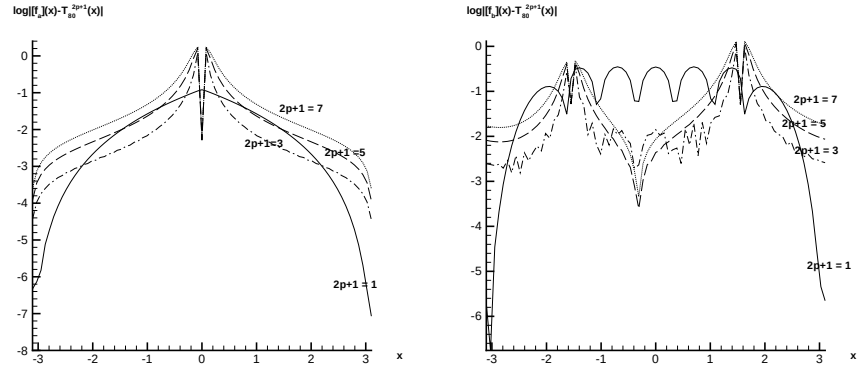

Figure 3.3: The logarithmic error of $\widetilde{T}_{80}^{\tau_{2p+1}}[f](x)$ with polynomial factor (3.7), $p = 0, 1, 2, 3$, for (a) $[f_a](x)$ and (b) $[f_b](x)$.

Figure 3.3 compares the logarithmic errors for the concentration method (3.1) with polynomial factors of various order. In the neighborhood of the discontinuities, the first order polynomial factor yields the best results, due to the strictly local nature of the method. We also note that convergence away from the discontinuities is not necessarily improved for higher order polynomial concentration factors, which is due to the global dependence of the polynomial based concentration detectors. Consequently, lower order factors may be more useful in calculation.

3.2. **Trigonometric factors: back to local differencing.** We now turn to our second family of *trigonometric* concentration factors. As shown in (3.10), the polynomial concentration factors (3.7) lead to higher order differentiation of the interpolant of the differences of $\Delta[f](x_{j+\frac{1}{2}})$. The

closely related trigonometric factors we consider below will amount to higher order *differences*, thus realizing in the dual Fourier space the (undivided) differences we discussed earlier in section 2. Thus, using the trigonometric factors discussed below we recover the local edge detectors in their dual space formulations. Indeed, we will arrive at an alternative approach for determining the scaling factor $q_{0,p}$ in (2.9) such that (2.10) is satisfied.

To demonstrate our point, we consider third-order differences, $\Delta^3 f_{j+\frac{1}{2}}$. We use the pseudo-spectral Fourier representation

$$f(x_j) = \sum_{k=-N}^{N} \widetilde{f}_k e^{ikx_j},$$

where $\widetilde{f}_k$ are the pseudo-spectral coefficients (3.2). After summation by parts, the third-order difference formula (2.4) reads

$$\begin{aligned}
\Delta^3 f_{j+\frac{1}{2}} &= \sum_{k=-N}^{N} \frac{1}{2N+1} \sum_{l=0}^{2N} f(x_l) e^{-ikx_l} \Big(- e^{ikx_{j+2}} + 3e^{ikx_{j+1}} - 3e^{ikx_j} + e^{ikx_{j-1}} \Big) \\
&= \frac{1}{2N+1} \sum_{l=0}^{2N} f(x_l) \sum_{k=-N}^{N} e^{ik(x_j - x_l)} \Big(- e^{ik2\Delta x} + 3e^{ik\Delta x} - 3 + e^{-ik\Delta x} \Big) \\
&= -\frac{2^4}{2N+1} \sum_{l=0}^{2N} f(x_l) \sum_{k=1}^{N} \sin^3 \frac{k\Delta x}{2} \sin k(x_{j+\frac{1}{2}} - x_{l+\frac{1}{2}}). \qquad (3.11)
\end{aligned}$$

Notice that the jump discontinuity is associated with a specific grid point value x_j, whereas in the similar global formula (3.4), no grid points are assigned.

The trigonometric identities

$$2\sin\frac{k\Delta x}{2}\cos kx_{l+\frac{1}{2}} = \sin kx_{l+1} - \sin kx_l, \qquad -2\sin\frac{k\Delta x}{2}\sin kx_{l+\frac{1}{2}} = \cos kx_{l+1} - \cos kx_l,$$

yield

$$\Delta^3 f(x_{j+\frac{1}{2}}) = \frac{2^3}{2N+1} \sum_{l=0}^{2N} \Big(f(x_{l+1}) - f(x_l) \Big) \sum_{k=1}^{N} \sin^2 \frac{k\Delta x}{2} \cos k(x_{j+\frac{1}{2}} - x_{l+\frac{1}{2}}). \qquad (3.12)$$

Therefore, the third order ($p = 1$) local edge detector method can be formulated in the dual space as

$$\Delta^3 f(x_{j+\frac{1}{2}}) = 2\widetilde{T}_N^{\tau_3}[f](x_{j+\frac{1}{2}}), \qquad (3.13)$$

where according to (3.5), $\widetilde{T}_N^{\tau_3}$ is associated with the concentration factors $\sigma_3(s) = c_3 4s\sin^2(\pi s/2)$ and $c_3 = \frac{1}{2}$ in agreement with $1/q_{0,1}$ in (2.8).Thus, $\widetilde{T}_N^{\tau_3}[f](x_{j+\frac{1}{2}})$ are nothing but the local differences $T^3[f](x_{j+\frac{1}{2}})$.

At this point it is instructive to show the consistency of the local and global approaches for derivation of the same edge detectors methods by computing the scaling factors c_p with the $q_{0,p}$'s derived in (2.9) from the global perspective. Comparing (3.13) and (3.5), we can determine the concentration factor $\sigma_3(k\Delta x/\pi)$ as

$$\sigma_3(s) = c_3 2^2 s\sin^2(\frac{\pi s}{2}). \qquad (3.14)$$

The admissibility condition in Corollary 3.1 requires the concentration factors to be normalized so that (3.4) holds, $\int_0^1 \sigma_3(s)ds/s = 1$ which dictates the value of c_3 as

$$c_3 \int_0^1 2^2 \sin^2\big(\frac{\pi s}{2}\big)ds = 1, \tag{3.15}$$

yielding $c_3 = \frac{1}{2}$, in agreement with $c_p = \frac{1}{q_{0,p}}$ for $p = 1$ in (2.8). A similar computation for higher order factors leads to

$$T_N^{\tau_{2p+1}}[f](x_{j+\frac{1}{2}}) = c_p \frac{2^{2p+1}}{N+1} \sum_{l=0}^{2N} (f(x_{l+\frac{1}{2}}) - f(x_l)) \sum_{k=1}^{N} \sin^{2p}\big(\frac{k\Delta x}{2}\big) \cos k(x_{j+\frac{1}{2}} - x_{l+\frac{1}{2}}). \tag{3.16}$$

Thus, the normalization

$$c_p \int_0^1 2^{2p} \sin^{2p}\big(\frac{\pi s}{2}\big)ds = 1, \tag{3.17}$$

yields

$$c_p = \frac{\sqrt{\pi}}{2^{2p}} \frac{\Gamma(2p+1)}{\Gamma(\frac{2p+1}{2})} = \frac{1}{\left(\begin{array}{c} 2p \\ p \end{array}\right)} = \frac{1}{q_{0,p}}, \tag{3.18}$$

in agreement with the derivation of the local edge detectors method (2.9). The general $(2p+1)$-order differencing then corresponds to the trigonometric factors

$$\sigma_{2p+1)}(s) = c_p 2^{2p} s \sin^{2p}\big(\frac{\pi s}{2}\big). \tag{3.19}$$

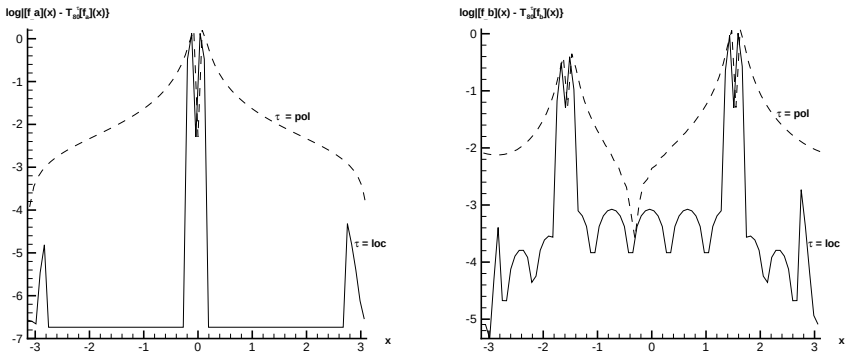

Figure 3.4: The logarithmic error of the fifth order (local) trigonometric vs the (global) polynomial factors $\widetilde{T}_{80}^{\tau_5}[f](x_j)$ applied to (a) $[f_a](x)$ and (b) $[f_b](x)$.

As exhibited in figure 3.4, the trigonometric edge detectors, (3.19), recover the regions of smoothness of a piecewise smooth function more accurately than the polynomial factors (3.7).

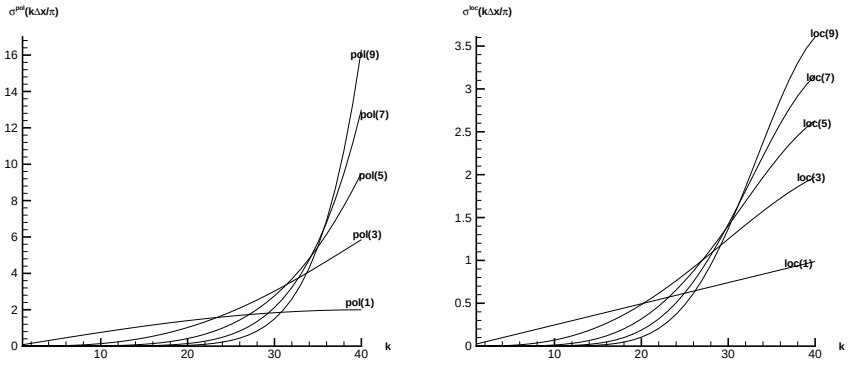

Figure 3.5: The concentration factors in spectral space using $N = 80$ for (a) the polynomial factors (3.7) and (b) the trigonometric factors (3.19).

Figure 3.5 compares the analogous concentration factors (3.7) and (3.19) for the polynomial and trigonometric edge detectors. As is evident from the comparison, both methods have increasing concentration factors on $[0, 1]$. Since both factors reduce the impact of the lower order modes while sharpening the contribution of the higher order modes, oscillations are inherent in the recovery of the jump function. The steeper slope of the concentration factor in the polynomial case results in more prevalent oscillations, suggesting that the application of a filter with polynomial edge detection method might effectively reduce the oscillations while still yielding high order convergence to zero away from the discontinuities.

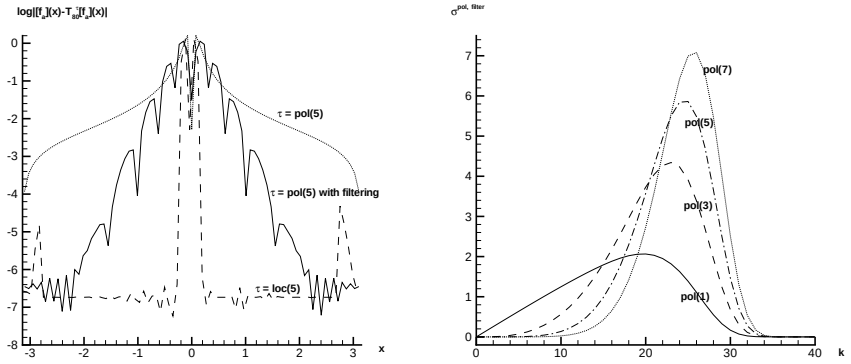

Figure 3.6: (a) Error graph for $[f_a](x)$ applying the concentration method with fifth order local, polynomial and filtered polynomial concentration factors. (b) Comparison of the filtered polynomial concentration factors (3.20 in spectral space shown for $k = 0, \cdots 40$.

For example, a filtered polynomial concentration factor

$$\sigma^{exp}_{2p+1}(s) = Const \cdot \sigma_{2p+1}(s) e^{-\alpha s^{\kappa}}, \tag{3.20}$$

where $Const$ is determined by the property (3.1), can help reduce oscillations and achieve higher accuracy away from the jump discontinuities. Figure 3.6 examines the application of (3.20) in both physical and spectral space. Here we choose filter parameters $\alpha = 32$ and $\kappa = 8$.

3.3. **Exponential concentration factors.** We close our list of examples for dual space detectors with a third family of concentration factors introduced in [7], where we introduced the *exponential* concentration factors,

$$\sigma^{exp}(\xi) = Const \cdot e^{\frac{1}{\gamma\xi(\xi-1)}}, \quad Const = \int_{\epsilon}^{1-\epsilon} exp(\frac{-1}{\gamma\xi(\xi-1)})d\xi. \tag{3.21}$$

They yield exponential convergence to zero away from the discontinuities with reduced oscillations everywhere except in the neighborhood of the jump discontinuities. We conclude by noting that the exponential concentration factor can be seen as the limiting case of high order p for the polynomial factors, with additional filtering to reduce the oscillations. It is then more powerful than the local methods in terms of convergence away from the discontinuities as well as localizing the neighborhood around the discontinuity

Figure 3.7(a) compares the different concentration factors, (3.7), (3.19) and (3.21). The error graph of example (2.2(a)) for the concentration method using the exponential factor is exhibited in figure 3.7(b).

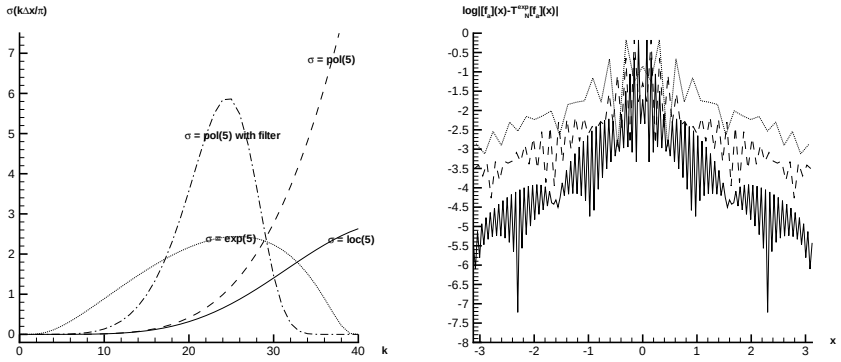

Figure 3.7: (a) Comparison of the exponential ($\gamma = 5$), polynomial, and trigonometric concentration factors in spectral space shown for $k = 0, \cdots 40$. (b) Error graph for $[f_a](x)$ applying the concentration method with (3.21), $\gamma = 5$ and $N = 40, 80$ and 160.

It is apparent from the discussion and figures above that the exponential factor both reduces oscillations and increases convergence away from a small neighborhood of the jump discontinuity. Both the higher order polynomial factors (3.7) in the global concentration method (3.1) and the local edge detection method (2.9) improve convergence rates away from the discontinuities, but decrease the accuracy in the neighborhoods of the jump. As is evident in figures 2.7 and 3.3, the neighborhoods surrounding the jump discontinuities tend to "spread out" as the order of the concentration factor (3.7) or (3.19) increases. The results within the neighborhood are slightly worse for the local edge detection method, as the spreading is dictated by (2.10) for the neighborhood around the jump discontinuity. Conversely, the neighborhoods around the jump discontinuities are not affected by the application of the concentration method using the first order polynomial concentration factor (3.8), or equivalently the first order local edge detection method (2.9). In this case, the convergence rate in the neighborhood of the discontinuities is $\mathcal{O}(\Delta x)$, but steep gradients elsewhere might be falsely identified as jump locations, since the convergence outside the neighborhood is also only $\mathcal{O}(\Delta x)$. If the discontinuities are located "far enough" apart, meaning that the jump function can be completely resolved,

then the exponential concentration factor is perhaps the most powerful of the methods, since $\widetilde{T}_N^{exp}[f](x) = \widetilde{T}_N[f](x) \to 0$ rapidly away from the discontinuities, and the oscillations appear only within a small neighborhood of the discontinuities. However, as will be seen in §4, interfering oscillations from "close" discontinuities can make it difficult to accurately recover the jump function.

3.4. **Enhanced edge detection.** While it is evident that the (local and global) edge detection methods converge to the singular support of a piecewise smooth function $f(x)$, the oscillations in the neighborhoods of the discontinuities and the various orders of convergence away from the discontinuities make it necessary to further enhance the results and "pinpoint" the jump discontinuity locations exactly. This has been achieved in [7] by separating the vanishing scales in the smooth regions from the $\mathcal{O}(1)$ scales in the neighborhoods of the jump discontinuities. Specifically, if $\{\xi_j\}_{j=1}^M$ denote the locations of the jump discontinuities of $f(x)$, then for admissible concentration factors in (3.1), the separation of scales is enhanced by computing, for some $q > 1$ at our disposal,

$$E_{q,N} := N^{q/2}(\widetilde{T}_N^{\tau}[f](x))^q \sim \begin{cases} N^{q/2}([f](\xi_j))^q, & \text{if } x = \xi_j, \\ \\ \mathcal{O}(N^{-q/2}), & \text{if } x \neq \xi_j, \end{cases}$$

leading to the enhanced concentration method,

$$E_N^{\tau}[f](x)) = \begin{cases} \widetilde{T}_N^{\tau}[f](x), & \text{if } |E_{q,N}| > J_{crit}, \\ \\ 0, & \text{if } |E_{q,N}| < J_{crit}. \end{cases} \tag{3.22}$$

Here J_{crit} is an $\mathcal{O}(1)$ global threshold parameter signifying the minimal amplitude below which jump discontinuities are neglected; after all, almost all grid values experience "jumps" and the question is their relative size relative w.r.t. the small scale of $1/N$. It is important to note that since (2.9) and (3.1) actually detect the neighborhoods of the jump discontinuities, $\mathcal{O}(\epsilon(N))$, rather than the discontinuities themselves, we use the nonlinear enhancement (3.22) in a window of $\mathcal{O}(\epsilon(N))$ to pinpoint the exact locations. Specifically, we determine that the exact discontinuities are where the largest amplitude $|E_{q,N}| > J_{crit}$ occur in each small neighborhood $\epsilon(N)$ of the jump discontinuities. Figure 3.8 show the powerful result of (3.22) in pinpointing the jump discontinuities.

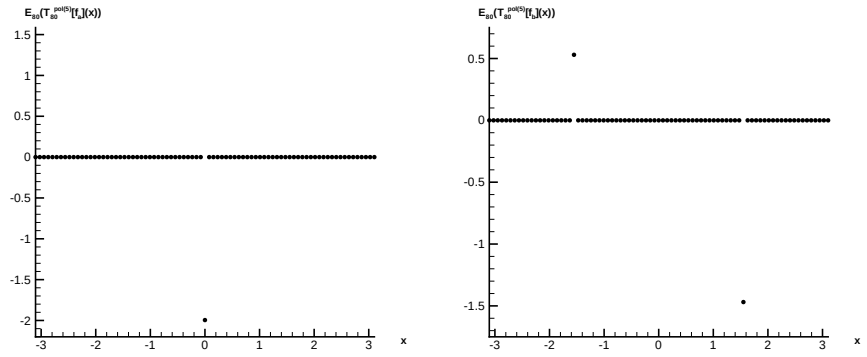

Figure 3.8: Application of (3.22) ($\widetilde{E}_{80}^{\tau_5}[f](x)$) to approximate (a) $[f_a](x)$ and (b) $[f_b](x)$.

This enhancement procedure requires an outside threshold parameter, reflecting the scaling of the function. This becomes an impediment for detecting edges in both small scale problems as well as problems with steep gradients and high variation. Additionally, pre-determination of the neighborhood value $\epsilon(N)$ is also necessary for (3.22), leading to the misidentification of jump discontinuities when they are located "too" close together. Next we address how to avoid the dependence on the outside threshold parameter.

4. MinMod edge detection

As is evident from the results in §2, both the global detectors based on high degree polynomials and, in particular, exponential factors, and local edge detectors based on low degree differencing, have the underlying feature that if the convergence rate is fast away from the neighborhoods of the discontinuities, then there are more oscillations in the neighborhood of the jump discontinuities. Hence it can be difficult to determine the true jump location. This is further complicated when jump discontinuities are located near to each other, since the oscillations occurring in the neighborhoods of each discontinuity interfere with the true jump discontinuities. As noted previously, the first order polynomial edge detection (3.8), or equivalently the first order local edge detection (2.9), does not yield oscillations in the neighborhoods of the discontinuities, but has slow convergence away from the discontinuities. On the other hand, the exponential concentration factor (3.21) produces rapid convergence to zero away from the neighborhoods of discontinuities, but suffers from severe oscillations within the neighborhoods. The loss of monotonicity with the increasing order is, of course, the canonical situation in many numerical algorithms. Here we introduce an adaptive edge detection procedure that realizes the strengths of both methods. We first observe that away from the jumps, one should let the exponentially small factors dominate by taking the *smallest* (in absolute) value between the low-order and high-order detectors. As we approach the jump discontinuity, the high-order produce spurious oscillations which should be rejected by the low-order detectors: hence, when two values disagree in sign, indicating spurious oscillations, the detectors should be set to zero. We end up with the so-called *minmod* limiter which plays a central role in non-oscillatory reconstruction of high-resolution methods for nonlinear conservation laws, (e.g., [10, 14] and the references therein),

$$\widetilde{T}_N^{minmod}[f](x) = minmod(\widetilde{T}_N^{\exp}[f](x), \widetilde{T}_N^{\tau_{2p+1}}[f](x)), \quad p = 1, 2, \cdots, \tag{4.1}$$

where the k-tuple *minmod* operation takes the form

$$minmod\{a_1, a_2, \dots, a_k\} := \begin{cases} s \cdot min\big(|a_1|, |a_2|, \dots, |a_k|\big) & \text{if } sgn(a_1) = \dots = sgn(a_k) := s \\ 0, & \text{otherwise.} \end{cases}$$

Here τ_{exp} is the discrete analog of the exponential concentration factors (3.21) and τ_{2p+1} represents the polynomial or trigonometric factors of order $(2p+1)$. Although the adaptive *minmod* algorithm is effective for any order polynomial, typically first order would be preferable. This adaptive algorithm can be extended to include other concentration factors, e.g.

$$\widetilde{T}_N^{mm}[f](x) = minmod(\widetilde{T}_N^{exp}[f](x), \widetilde{T}_N^{poly}[f](x), \widetilde{T}_N^{trig}[f](x)), \tag{4.2}$$

for any odd order of polynomial and trigonometric factors. For simplicity, we use the *minmod* algorithm as described in (4.1) with the first and third order polynomial factors (3.7). Figure 4.1 illustrates the improvement in using (4.1). While some residual oscillations remain in figure

4.1(a), it is clear that if the *minmod* is followed by the nonlinear enhancement procedure (3.22) the outside scaling parameter becomes less significant in determining the jump locations, as shown in figure 4.1(b).

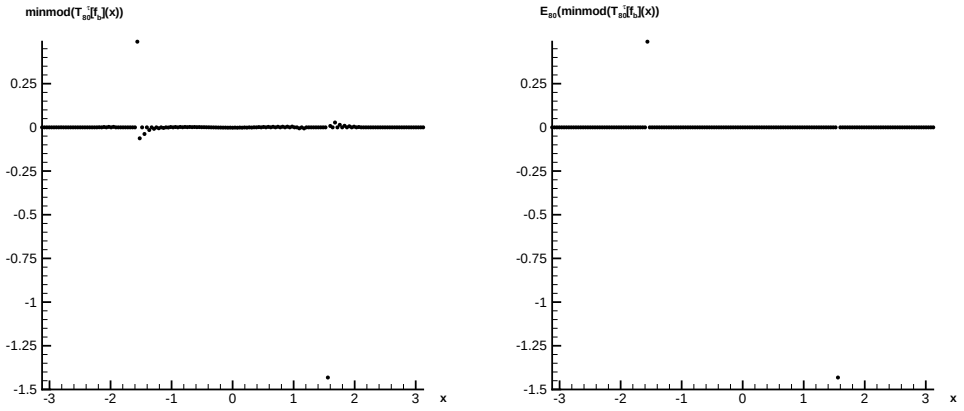

Figure 4.1: (a) The *minmod* algorithm (4.1) applied to example 2.2(b) and (b) with the nonlinear enhancement using 80 Fourier modes.

Furthermore, the *minmod* algorithm works even when the jump discontinuities are located close together. As an example, consider the jump function and associated jump function exhibited in figure 4.2.

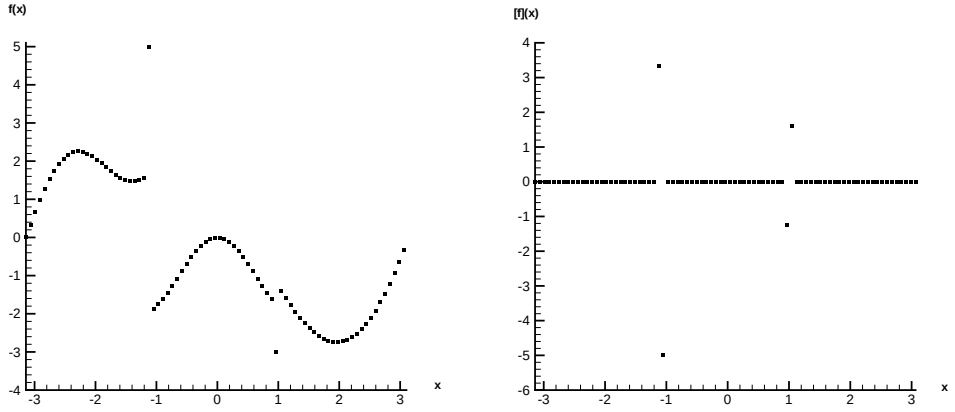

Figure 4.2: (a) An example of a piecewise smooth function on $N = 80$ points and (b) the jump function.

Figure 4.3 compares the results of application of the concentration method (3.1) with various concentration factors and the *minmod* algorithm. It is evident that the polynomial factor τ_{2p+1} does not converge to zero fast enough away from the discontinuities, hence the steep gradients of the function might be misinterpreted as jump discontinuities. On the other hand, the concentration method using τ_{exp} causes interfering oscillations in the neighborhoods of the discontinuities, making it difficult to determine where the true jumps are. The *minmod* algorithm (4.1) ensures the convergence to the jump function without interference of the oscillations.

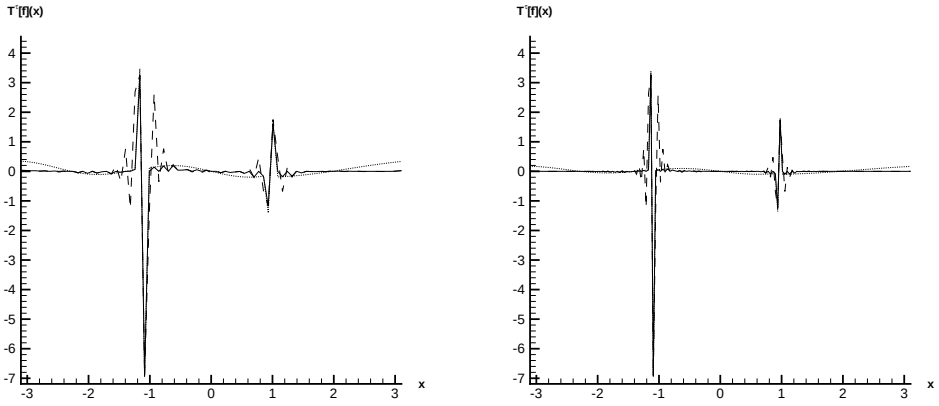

Figure 4.3: Edge detection using first order τ_{pol} (dotted), τ_{exp} (dashed) and the *minmod* algorithm (solid) with (a) 80 and (b) 160 points.

At this point, the application of the enhancement procedure introduced in [7] works directly to pinpoint the jump discontinuities, *without* having to determine a neighborhood parameter $\epsilon(N)$. Furthermore, one can apply the minimization algorithm discussed in [1] and [2] to reduce the $\mathcal{O}(\Delta x)$ error in the approximation of the amplitude of the jump discontinuity.

5. Numerical applications

In this section we describe some two dimensional applications using the *minmod* edge detection algorithm (4.1). In each case, the adaptive edge detection method is performed one dimension at a time and is followed by the enhancement procedure (3.22).

One important application of edge detection is in the segmentation process associated with magnetic resonance imaging (MRI). Specifically, analyst are interested in study particular regions of the brain, and edge detection can be effectively employed to extract or "segment" out a region of interest. The classical example of the Shepp-Logan phantom image, displayed in figure 5.1, is a typical initial test to determine efficacy of imaging techniques [13].

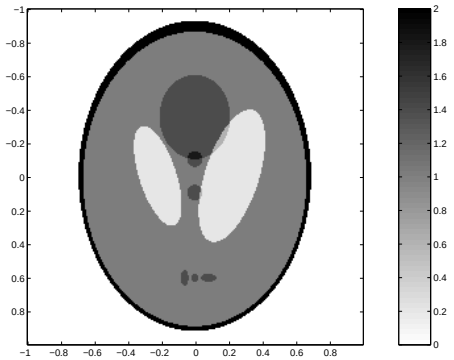

Figure 5.1: Contour plot of the Shepp-Logan brain image.

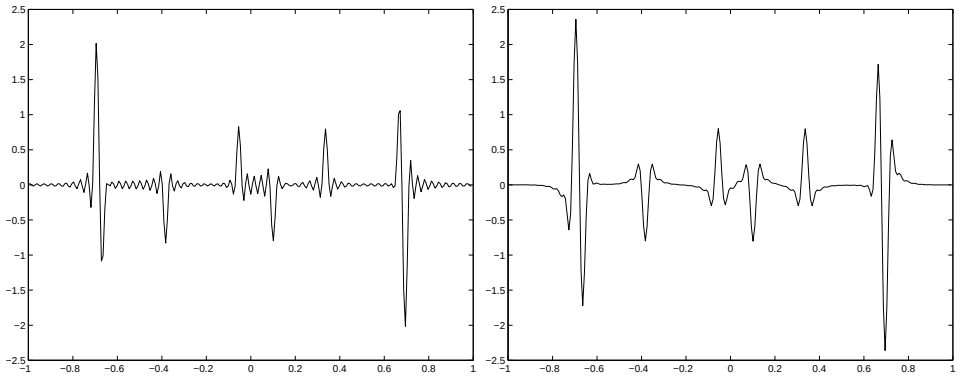

Figure 5.2: The concentration method (3.1) applied to the Shepp-Logan phantom on $[128 \times 128]$ points using (a) the polynomial concentration factor (3.7) and (b) the exponential concentration factor (3.21) at the cross section $(x, 0)$.

Figure 5.2 exhibits the application of the concentration method (3.1) applied using the concentration factors (3.7) and (3.21) for a one dimensional cross section of the image. What is evident in figure 5.2 is that the different concentration factors yield different convergence patterns in the smooth regions of the image.

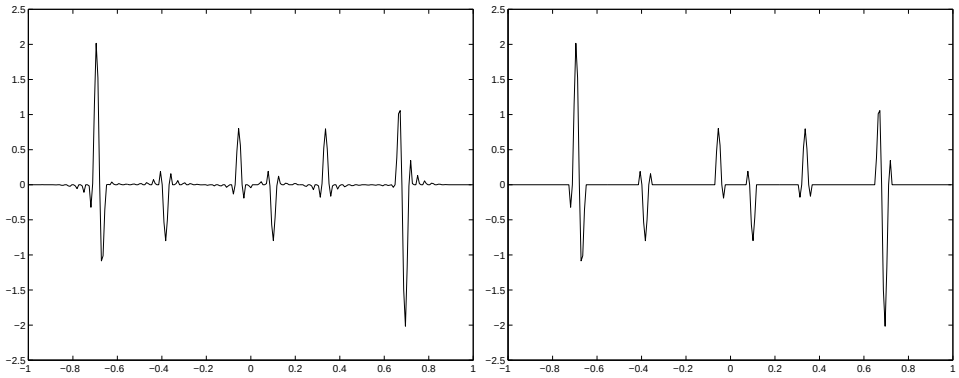

Figure 5.3: The *minmod* procedure (4.1) applied to the Shepp-Logan brain phantom (a) at the cross section $(x, 0)$ and (b) with nonlinear enhancement (3.22).

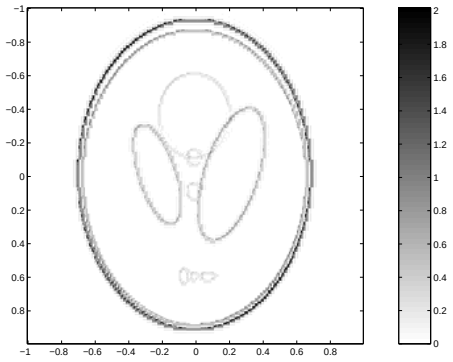

Figure 5.4: The nonlinear enhancement procedure (3.22) applied to the Shepp-Logan brain phantom image.

As exhibited in figures 5.3 and 5.4, application of the *minmod* algorithm (4.1), further enhanced by (3.22), enables complete segmentation of the images.

Let us now consider an example of a real image, a transversal slice of a human brain provided by the Gabrieli Lab [3], exhibited in figure 5.5.

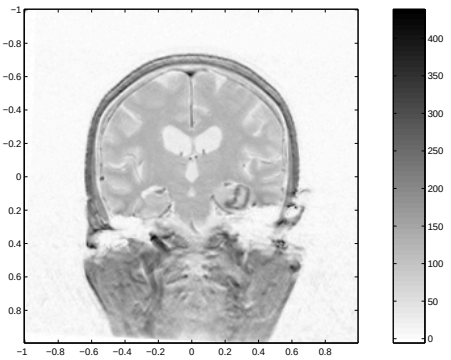

Figure 5.5: Contour plot of the Gabrieli brain image.

Since the data is real, random noise is prevalent throughout the image. An outside scaling parameter is introduced to help distinguish noise from true image data in the Gabrieli brain image figures. A discussion of how the effects of noise is reduced on the concentration method (3.1) can be found in [2]. Figure 5.6 displays the concentration method (3.1) applied to the Gabrieli image on a one dimensional cross section using the first order polynomial (3.7) and exponential (3.21) concentration factors. As exhibited in figure 5.7(a), the *minmod* algorithm improves the results by "adapting" the concentration method. The nonlinear enhancement procedure (3.22), shown in figures 5.7(b) and 5.8(a), completes the clarification of the distinct structures of the Gabrieli image.

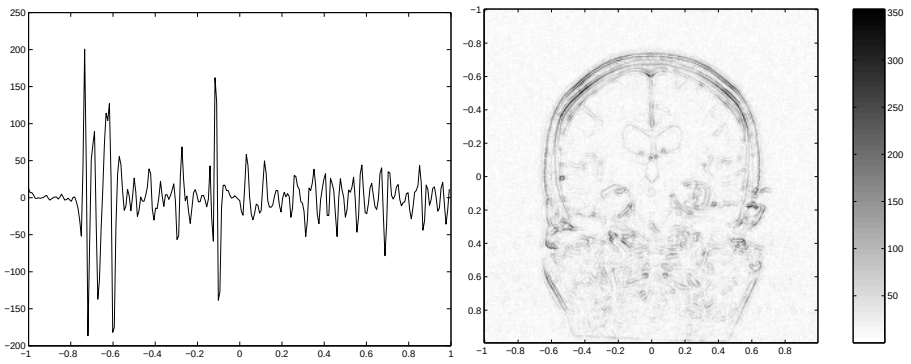

Figure 5.6: The concentration method (3.1) applied to the Gabrieli image using (a) the first order polynomial concentration factor (3.7) and (b) the exponential concentration factor (3.21) at the cross section $(x, 0)$.

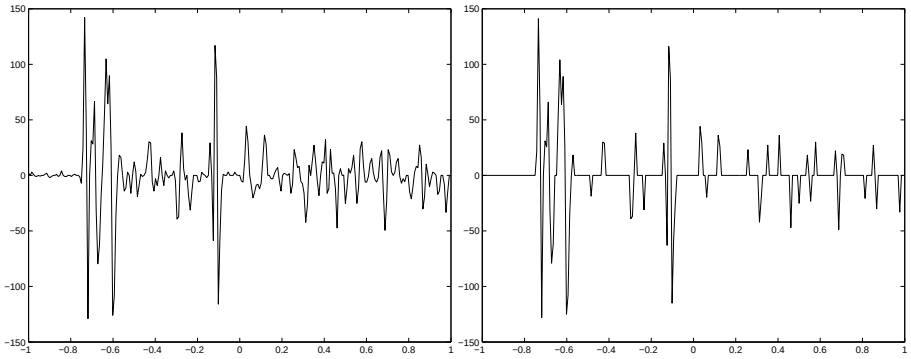

Figure 5.7: Edge detection of the Gabrieli image by applying the (a) *minmod* algorithm (4.1) (b) *minmod* and nonlinear enhancement (3.22) procedures at the cross section $(x, 0)$.

Finally, we see in figure 5.8(b) that the *minmod* (4.1) and nonlinear enhancement procedures (3.22) enables high resolution reconstruction of the Gabrieli lab MRI via the Gegenbauer reconstruction procedure [9].

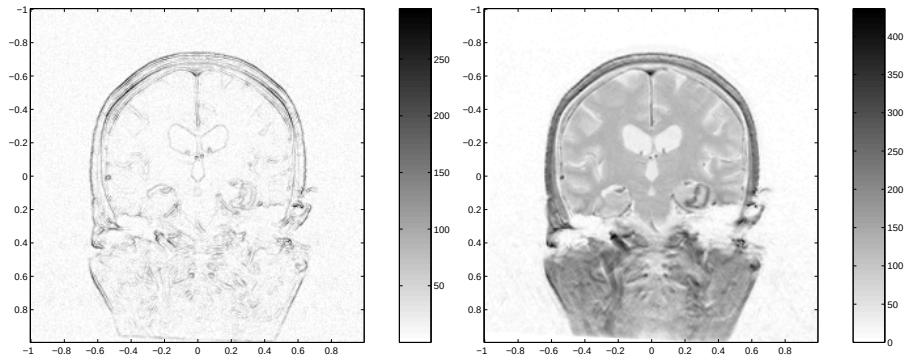

Figure 5.8: Contour plot of the (a) edge detection of the Gabrieli image by applying the *minmod* and nonlinear enhancement procedures one dimension at a time. (b) Gegenbauer reconstruction after the edges have been located.

6. Conclusion

In this paper we provide a complete description of edge detection from both the physical and spectral data view points. As discussed in §3, the local and global edge detection method are consistent in their approaches. The *minmod* procedure (4.1) provides a computationally efficient and robust method to produce edges of images *without* the need of any outside scaling parameters. Thus, the nonlinear enhancement procedure (3.22) works efficiently to "pinpoint" the edges of an image. The numerical results given throughout this paper and specifically in §5 demonstrate the efficacy of our method, particularly in its ability to enable high resolution reconstruction and the segmentation of images.

References

[1] R. Archibald and A. Gelb, Reducing the Effects of Noise in Image Reconstruction, *J. Sci. Comp.,* **17** (1-4), 167-180, (2002).

[2] R. Archibald and A. Gelb, A Method to Reduce the Gibbs Ringing Artifact in MRI Scans While Keeping Tissue Boundary Integrity, *IEEE Transactions on Medical Imaging*, **21** (4), (2002).

[3] Brainiac, Scanning and Analysis Resources, Gabrieli Lab, Stanford University, http://gablab.stanford.edu/brainiac.
[4] B. Fornberg, A Practical Guide to Pseudospectral Methods, Cambridge University Press, 1996.
[5] K.S. Eckhoff, Accurate reconstructions of functions of finite regularity from truncated series expansions, *Math. Comp.* **64**, 671-690 (1995).
[6] A. Gelb and E. Tadmor, Detection of edges in spectral data, Appl. Comp. Harmonic Anal., **7** 101-135 (1999).
[7] A. Gelb and E. Tadmor, Detection of edges in spectral data II. Nonlinear Enhancement, *SIAM J. Numer. Anal.*, **38**, 1389-1408, (2001).
[8] A. Gelb and E. Tadmor, Spectral Reconstruction of Piecewise Smooth Functions from Their Discrete Data, *Mathmatical Modelling and Numerical Analysis,* **36** (2), 155-175 (2002).
[9] D. Gottlieb and C.-W. Shu, On the Gibbs phenomenon and its resolution, SIAM Review, 1997.
[10] A. Harten, *High resolution schemes for hyperbolic conservation laws*, J. Comput. Phys. 49 (1983), 357–393.
[11] A. Jeffrey, Handbook of Mathematical Formulas and Integrals, Academic Press, 1995.
[12] G. Kvernadze, Determination of the jump of a bounded function by its Fourier series, J. Approx. Theory, **92**, 167-190, (1998).
[13] Z. Liang and P. Lauterbur, (2000), *Principles of Magnetic Resonance Imaging, a Signal Processing Perspective*, IEEE Press.
[14] E. Tadmor, *Approximate solutions of nonlinear conservation laws*, in "Advanced Numerical Approximation of Nonlinear Hyperbolic Equations" Lecture notes in Mathematics **1697**, 1997 C.I.M.E. course in Cetraro, Italy, (A. Quarteroni ed.) Springer Verlag, 1-149 (1998).
[15] E. Tadmor & J. Tanner, *Adaptive mollifiers – high resolution recovery of piecewise smooth data from its spectral information* Foundations Comput. Math. 2(2) **155-189**, (2002).
[16] E. Tadmor & J. Tanner, *Adaptive filters for piecewise smooth spectral data*, IMA J. Numer. Anal., to appear.

Department of Mathematics and Statistics, P.O. Box 871804 Arizona State University Tempe, AZ 85287-1804.

E-mail address: ag@math.la.asu.edu

Department of Mathematics, Center of Scientific Computation And Mathematical Modeling (CSCAMM) and Institute for Physical Science and Technology (IPST), University of Maryland, MD 20742.

E-mail address: tadmor@cscamm.umd.edu